Paleoceanography and Paleoclimatology

RESEARCH ARTICLE
10.1029/2020PA004063

Ice Age-Holocene Similarity of Foraminifera-Bound Nitrogen Isotope Ratios in the Eastern Equatorial Pacific

Anja S. Studer[1,2], Figen Mekik[3], Haojia Ren[4], Mathis P. Hain[5], Sergey Oleynik[6], Alfredo Martínez-García[2], Gerald H. Haug[2,7], and Daniel M. Sigman[6]

[1]Department of Environmental Sciences, University of Basel, Basel, Switzerland, [2]Max Planck Institute for Chemistry, Climate Geochemistry Department, Mainz, Germany, [3]Department of Geology, Grand Valley State University, Allendale, MI, USA, [4]Department of Geosciences, National Taiwan University, Taipei, Taiwan, [5]University of California, Earth and Planetary Sciences Department, Santa Cruz, CA, USA, [6]Department of Geosciences, Princeton University, Princeton, NJ, USA, [7]ETH Zurich, Geological Institute, Zurich, Switzerland

Key Points:

- Foraminifera-bound $\delta^{15}N$ was similar during the last ice age and the Holocene in the eastern equatorial Pacific, unlike bulk sedimentary $\delta^{15}N$
- Bulk sediment $\delta^{15}N$ is likely biased to lower ice age values by foreign N inputs and weaker sedimentary diagenesis
- The foraminifera-bound $\delta^{15}N$ data may reflect that water column denitrification was not reduced during the last glacial period

Supporting Information:

Supporting Information may be found in the online version of this article.

Correspondence to:

A. S. Studer,
anja.studer@unibas.ch

Citation:

Studer, A. S., Mekik, F., Ren, H., Hain, M. P., Oleynik, S., Martínez-García, A., et al. (2021). Ice Age-Holocene similarity of foraminifera-bound nitrogen isotope ratios in the eastern equatorial Pacific. *Paleoceanography and Paleoclimatology*, *36*, e2020PA004063. https://doi.org/10.1029/2020PA004063

Received 27 JUL 2020
Accepted 14 APR 2021

Abstract Bulk sediment $\delta^{15}N$ records from the eastern tropical Pacific (ETP) extending back to the last ice age most often show low glacial $\delta^{15}N$, then a deglacial $\delta^{15}N$ maximum, followed by a gradual decline to a late Holocene $\delta^{15}N$ that is typically higher than that of the Last Glacial Maximum (LGM). The lower $\delta^{15}N$ of the LGM has been interpreted to reflect an ice age reduction in water column denitrification. We report foraminifera shell-bound nitrogen isotope (FB-$\delta^{15}N$) measurements for the two species *Neogloboquadrina dutertrei* and *Neogloboquadrina incompta* over the last 35 ka in two sediment cores from the eastern equatorial Pacific (EEP), both of which have the typical LGM-to-Holocene increase in bulk sediment $\delta^{15}N$. FB-$\delta^{15}N$ contrasts with bulk sediment $\delta^{15}N$ by not indicating a lower $\delta^{15}N$ during the LGM. Instead, the FB-$\delta^{15}N$ records are dominated by a deglacial $\delta^{15}N$ maximum, with comparable LGM and Holocene values. The lower LGM $\delta^{15}N$ of the bulk sediment records may be an artifact, possibly related to greater exogenous N inputs and/or weaker sedimentary diagenesis during the LGM. The new data raise the possibility that the previously inferred glacial reduction in ETP water column denitrification was incorrect. A review of reconstructed ice age conditions and geochemical box model output provides mechanistic support for this possibility. However, equatorial ocean circulation and nitrate-rich surface water overlying both core sites allow for other possible interpretations, calling for replication at non-equatorial ETP sites.

Plain Language Summary The $^{15}N/^{14}N$ ratio of sediments provides information on the past marine nitrogen (N) cycle through the production of N-bearing organic matter in the surface ocean and its burial in the sediments. Previous measurements of the sedimentary $^{15}N/^{14}N$ ratio in the eastern equatorial Pacific (EEP) indicate lower values during the last ice age compared to the Holocene (the current warm period). This has been interpreted to reflect an ice age reduction in the oceanic N loss process known as "denitrification" that occurs between 200 and 500 m depth in this region of the ocean. However, the $^{15}N/^{14}N$ ratio measured on the whole sediment can be biased by biological and chemical processes in the sediments and by foreign N inputs. To avoid these complications, we measured the $^{15}N/^{14}N$ ratio of organic N embedded in the calcite shell of unicellular zooplankton (foraminifera) in two sediment cores from the EEP. We found similar foraminifera-bound $^{15}N/^{14}N$ ratios during the last ice and the Holocene. This may argue against the long-held interpretation of a reduction in denitrification during the last ice age. However, the oceanographic setting of these equatorial cores leaves open alternative interpretations, calling for further work at other eastern tropical Pacific sites.

1. Introduction

The eastern tropical Pacific (ETP) is important in climate and biogeochemical cycles. It hosts three upwelling systems: the equatorial upwelling, the coastal upwelling off California in the eastern tropical North Pacific (ETNP), and the Peru-Chile coastal upwelling in the eastern tropical South Pacific (ETSP) (Figure 1). In these regions, cold, nutrient-rich waters upwell to the surface, fueling productivity. In addition, slow circulation through the thermocline in these regions isolates the mid-depths waters from ventilation by the high latitudes. Due to the combination of slow ventilation and the abundance of sinking organic matter, respiration completely consumes the supply of dissolved oxygen (O_2), producing O_2-deficient zones (ODZs),

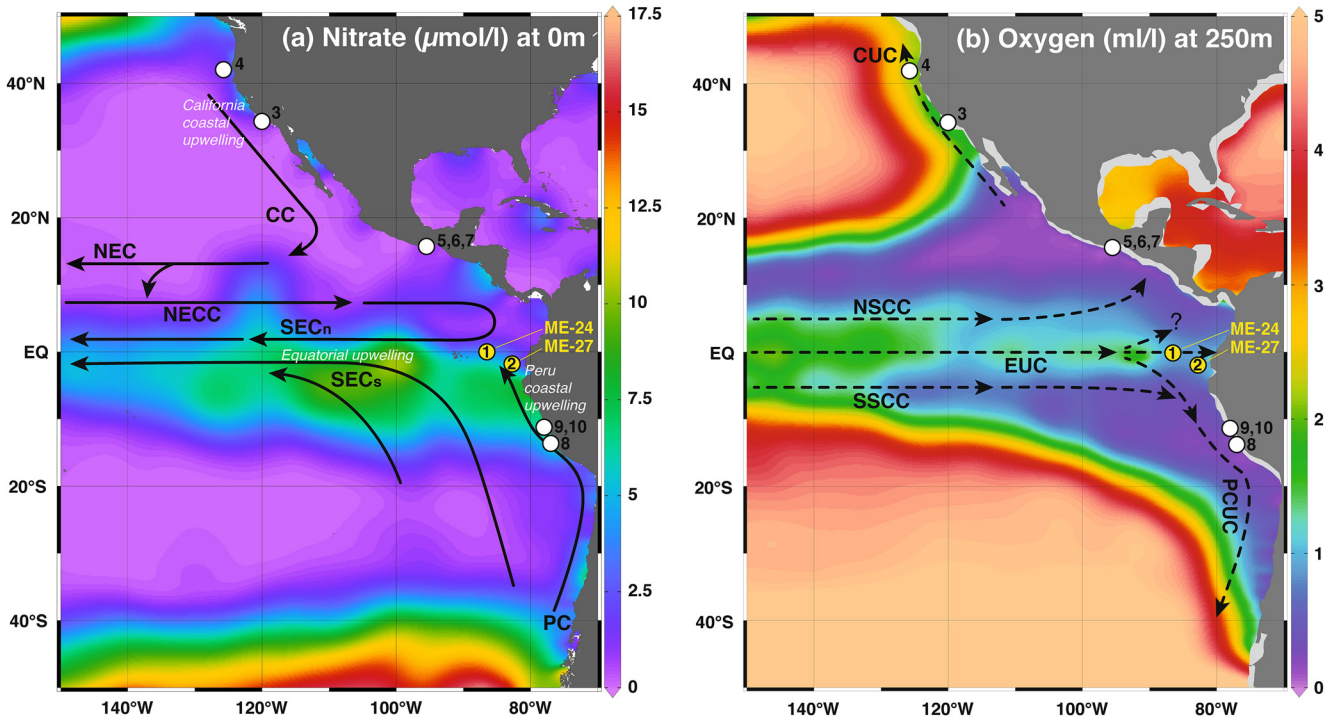

Figure 1. Modern oceanographic context of the sediment cores used for FB-$\delta^{15}N$ reconstruction. Circulation in the surface (solid lines in a) and shallow subsurface (dashed lines in b) in the ETP, overlain on mean annual nitrate concentrations at the surface (a) and mean annual oxygen concentrations at 250 m depth (b) (Garcia et al., 2010a). The core sites of this study are in yellow, and cores referred to in the text are in white: (1) ME-24, (2), ME-27, (3) ODP 893, (4) W8709-13PC, (5) MD02-2520, (6) ME-05A-11PC, (7) ME-05A-03JC, (8) W7706-37, (9) W7706-40, (10) W7706-41. CC, California Current, NEC, North Equatorial Current, NECC, North Equatorial Countercurrent, SEC, South Equatorial Current (with the lowercase letters n and s indicating northern and southern branch, respectively), PC, Peru-Chile Current, CUC, California Undercurrent, EUC, Equatorial Undercurrent, NSCC, Northern Subsurface Countercurrent, SSCC, Southern Subsurface Countercurrent, PCUC, Peru-Chile Undercurrent. The circulation was drawn after Wyrtki (1966), Kessler et al. (2006), Talley et al. (2011), and S. Zheng et al. (2016). The maps were generated with Ocean Data View (Schlitzer, 2002).

one in the ETNP and one in the ETSP. Within the ODZs, denitrification reduces nitrate to N_2, providing the oxidant for the respiration of organic matter. This water column denitrification is a major driver of fixed N loss from the ocean (Deutsch et al., 2001), and it can also produce nitrous oxide, a potent greenhouse gas, as a side-product (Pierotti & Rasmussen, 1980). Moreover, reconstruction of the history of denitrification may provide insight into past changes in ocean circulation and the strength of the global ocean's biological carbon pump (Altabet et al., 1995, 2002; Ganeshram et al., 1995; Martinez et al., 2006; Robinson et al., 2007).

During denitrification, ^{14}N-nitrate is preferentially lost from the ocean water column, elevating the residual nitrate in $\delta^{15}N$ (Cline & Kaplan, 1975; Liu & Kaplan, 1989) (with $\delta^{15}N = [(^{15}N/^{14}N)_{sample}/(^{15}N/^{14}N)_{atm\ N2} - 1]*1000‰$). This ^{15}N-enriched nitrate is then transported laterally in the subsurface, spreading this isotopic signal through the mid-depth ocean. The high-$\delta^{15}N$ nitrate is also supplied to the surface by upwelling, resulting in the production of high-$\delta^{15}N$ organic matter. This organic N is then exported to depth, possibly after significant lateral transport in the surface. Regeneration back to nitrate in the subsurface represents an additional mechanism for spreading the high-$\delta^{15}N$ signal of denitrification both laterally and vertically (Sigman et al., 2009).

The water from the ETNP with its ^{15}N-enriched nitrate is transported northward in the subsurface with the California Undercurrent (CUC) and southward at the surface with the California Current (CC) (Figure 1) (S. S. Kienast et al., 2002; Sigman et al., 2005). In the tropical Pacific, the CC flows into the North Equatorial Current (NEC), which itself recirculates into the North Equatorial Counter Current (NECC). The NECC is one of a number of inputs to the Equatorial Undercurrent (EUC), and the EUC is a major source water for equatorial upwelling (Goodman et al., 2005; Kessler, 2006; Talley et al., 2011; Wyrtki, 1966). Water from the ETSP with its elevated nitrate $\delta^{15}N$ is transported southward in the subsurface with the Peru-Chile Undercurrent (PCUC) (De Pol-Holz et al., 2009) and northward in the surface with the Peru-Chile Current (PC)

(Lukas, 1986; Silva & Neshyba, 1979). The high-$\delta^{15}N$ signal of ETSP denitrification is thus advected to the southern part of the eastern equatorial Pacific (EEP) upwelling, and it may also be transported further west with the South Equatorial Current (SEC) (Peters et al., 2018; Rafter et al., 2012; Rafter & Sigman, 2016).

A second N isotope signal that pertains to the EEP (as well as to the central equatorial Pacific) is that of partial nitrate consumption in surface waters (Altabet, 2001; Altabet and François, 1994). The preferential consumption of ^{14}N nitrate by phytoplankton produces low-$\delta^{15}N$ organic matter above the upwellings and leaves the residual nitrate enriched in ^{15}N. The high-$\delta^{15}N$ nitrate is then advected away from the upwelling, with continued consumption leading to the production of high-$\delta^{15}N$ organic matter (Altabet & François, 1994). This pattern is reflected in the $\delta^{15}N$ of bulk organic matter and foraminifera shell-bound organic matter on the seabed (Costa et al., 2016; Farrell et al., 1995). Sediment records of the N isotopes in the EEP are thus expected to record changes in both water column denitrification and the spatial pattern of surface nitrate consumption.

A third potential influence is the $\delta^{15}N$ of shallow subsurface nitrate imported into the EEP by the equatorial system. Nitrate $\delta^{15}N$ data are lacking in the EEP east of the Galapagos Islands. West of Galapagos, the $\delta^{15}N$ of nitrate in the EUC proper is ~7.1‰, similar to that of Subantarctic Mode Water, which is the ultimate nitrate source to much of the tropical Pacific thermocline (Rafter et al., 2012). Strengthening in the flow of the EUC has the potential to lower the $\delta^{15}N$ of the nitrate supply to the EEP relative to that supplied from the denitrification zones. However, the caveat must be added that the EUC flow is interrupted by the Galapagos, and thus its nitrate isotopic signature may not persist east of the islands. This must be clarified by future nitrate isotope studies.

A water mass known as the subsurface equatorial "thermostad" just below the EUC as well as the eastward-flowing Southern Subsurface Counter Current (SSCC) have a nitrate $\delta^{15}N$ that can reach below 6‰ (Rafter et al., 2012; Rafter & Sigman, 2016). This lower nitrate $\delta^{15}N$ results from the remineralization of low-$\delta^{15}N$ sinking N associated with the upwelling and incomplete consumption of nitrate that upwells along the equator and its southern margin. Thus, rather than being a distinct signal of nitrate source from the west, the lower nitrate $\delta^{15}N$ of the thermostad and SSCC is an additional aspect of the signal of incomplete nitrate consumption in the equatorial Pacific. Accordingly, its likely effect is to amplify the $\delta^{15}N$ lowering of sinking N due to incomplete nitrate consumption in the region.

Existing bulk sediment $\delta^{15}N$ records from the ETNP, ETSP, and EEP typically show low glacial $\delta^{15}N$ that is followed by a deglacial $\delta^{15}N$ rise (De Pol-Holz et al., 2006; Dubois et al., 2011; Emmer & Thunell, 2000; Farrell et al., 1995; Ganeshram et al, 1995, 2000; Hendy et al., 2004; Hendy & Pedersen, 2006; Higginson & Altabet, 2004; S. S. Kienast et al., 2002; Pichevin et al., 2010; Pride et al., 1999; Robinson et al., 2007, 2009; Thunell & Kepple, 2004). This $\delta^{15}N$ increase is widely interpreted as a deglacial rise in water column denitrification across the ETP, an interpretation supported by a comparable deglacial $\delta^{15}N$ rise in the Arabian Sea of the Indian Ocean (Altabet et al., 2002; Ganeshram et al., 2000). Typically, in the ETSP, the $\delta^{15}N$ rise is observed to begin at ~17–18 ka, in step with southern hemisphere warming (De Pol-Holz et al., 2006; Higginson & Altabet, 2004; Robinson et al., 2007), whereas the $\delta^{15}N$ rise in the ETNP (and downstream of it) occurs with the first abrupt northern hemisphere warming at ~14–15 ka, associated with the Northern Hemisphere's Bolling-Allerod Warm Period (Chang et al., 2014, 2008; Emmer & Thunell, 2000; S. S. Kienast et al., 2002; Pride et al., 1999). The deglacial rises in water column denitrification in the ETNP and ETSP, with their respective timings, are often interpreted as the result of a tendency for warming to enhance water column suboxia and denitrification, through the decreased solubility of O_2 and/or slower ventilation of intermediate waters and the thermocline under warmer climate (Galbraith et al., 2004). A deglacial rise in nutrient supply to the thermocline has also been implicated, the concept being that increased thermocline nutrients would drive higher lower latitude export production and thus more oxygen demand for respiration in the thermocline (Robinson et al., 2005). Millennial scale variations during the deglaciation are largely consistent with these interpreted mechanisms (Robinson et al., 2007).

In many ETP records, the later deglaciation and Holocene is characterized by a subsequent decline in bulk sediment $\delta^{15}N$. In some records, the decline is minor; in others, the decline almost completely compensates for the more abrupt early deglacial $\delta^{15}N$ rise. There have been multiple plausible interpretations of this decline: as part of a whole-ocean trend in nitrate $\delta^{15}N$, a late deglacial decline in water column denitrification,

and/or a rise in N_2 fixation (Deutsch et al., 2004; Galbraith et al., 2013; Thunell & Kepple, 2004). The deglacial $\delta^{15}N$ maximum is often accompanied by deglacial maxima in redox sensitive trace metals and/or sediment lamination (Pride et al., 1999; Y. Zheng et al., 2000). These parallel changes support the interpretation of the deglacial $\delta^{15}N$ maximum as due to an associated temporal peak in water column denitrification. However, as with the $\delta^{15}N$ records, the Holocene evolution of trace metal concentrations and lamination varies among sediment cores, declining back to baseline in some but not in others (Chang et al., 2014; Muratli et al., 2010; Y. Zheng et al., 2000). Finally, the deglacial $\delta^{15}N$ maximum itself has significantly different temporal structure in different regions and sediment cores (De Pol-Holz et al., 2006; Dubois et al., 2011; Emmer & Thunell, 2000; Ganeshram et al., 2000; Hendy & Pedersen, 2006; Higginson & Altabet, 2004; S. S. Kienast et al., 2002; Pichevin et al., 2010; Robinson et al., 2009, 2007; Thunell & Kepple, 2004).

In the EEP, the LGM-to-Holocene $\delta^{15}N$ rise in the first sediment $\delta^{15}N$ records was initially interpreted as a lower degree of nitrate consumption during the ice ages (Farrell et al., 1995). However, the change was very similar to that reconstructed from the ETP (Ganeshram et al., 1995); as described above, that change has been interpreted as deriving from an increase in water column denitrification. The LGM-to-Holocene sediment $\delta^{15}N$ rise in the EEP is now most often interpreted as a shared ETP/EEP signal, reflecting a rise in the $\delta^{15}N$ of subsurface nitrate as a result of an LGM-to-Holocene increase in water column denitrification (Dubois et al., 2011). Further west in the EEP, studies have revealed no LGM-to-Holocene rise in sediment $\delta^{15}N$ but rather a deglacial maximum, which is also apparently observed in the western equatorial Pacific (Rafter & Charles, 2012). This sediment $\delta^{15}N$ signal might be linked to the deglacial $\delta^{15}N$ maximum that is apparent in some records from the ETP. Differencing of western and eastern equatorial Pacific sediment $\delta^{15}N$ records yields a signal with orbital periodicities, dominantly of precession; this has been interpreted as a changing degree of nitrate consumption that results from insolation-driven EEP upwelling changes (Rafter & Charles, 2012). Interpretations aside, sediment $\delta^{15}N$ records from the EEP appear to hold signals of both an LGM-to-Holocene sediment $\delta^{15}N$ rise and, further westward, a deglacial $\delta^{15}N$ maximum.

The existing $\delta^{15}N$ records mentioned above are all based on N isotopic measurement of the bulk sediment ($\delta^{15}N_{bulk}$). However, the primary N isotopic signals acquired in the surface ocean may be obfuscated in $\delta^{15}N_{bulk}$. Two causes for this are (1) diagenetic alteration during sinking in the water column and early burial in the sediment (Altabet and François, 1994), and (2) the contribution of organic and inorganic N derived from terrestrial or distal marine (e.g., shelf) sources (Meckler et al., 2011; Schubert & Calvert, 2001). To avoid these biases, recent work has focused on measuring the $\delta^{15}N$ of organic matter bound within and protected by the tests of microfossils, such as foraminifera and diatoms (Ren et al., 2009; Robinson et al., 2004).

Here, we report measurements of foraminifera shell-bound $\delta^{15}N$ (FB-$\delta^{15}N$) on the two species *Neogloboquadrina dutertrei* and *Neogloboquadrina incompta* (formerly named *Neogloboquadrina pachyderma* (dextral); Darling et al., 2006) in two sediment cores extending back to the last ice age. These cores (ME0005-24JC and ME0005-27JC) fall within the nutrient-rich EEP (Figure 1). They both have abundant foraminifera and a rich set of previous measurements. Of particular interest, each core shows a LGM-to-Holocene increase in bulk sediment $\delta^{15}N$ similar to that observed at other EEP and ETP sites, which has most often been interpreted as indicating that ETP water column denitrification was reduced during the LGM (De Pol-Holz et al., 2006, 2007; Dubois & Kienast, 2011; Ganeshram et al., 1995, 2000; Robinson et al., 2007).

2. Materials and Methods

Sediment cores ME0005-24JC and ME0005-27JC (hereafter abbreviated as ME-24 and ME-27) were retrieved from the EEP. ME-24 is located north of Carnegie Ridge (0°1.3′ N, 86°27.8′ W, 2941 m), while ME-27 is located south of Carnegie Ridge (1°51.2′ S, 82°47.2′ W, 2203 m) (Figure 1). The age models for both sediment cores have been updated by Dubois et al. (2014) and are based on (1) radiocarbon ages measured on the planktonic foraminifera *N. dutertrei* by accelerator mass spectrometry (S. S. Kienast et al., 2007; Kusch et al., 2010), (2) correlation of benthic foraminifera oxygen isotopes to the LR04 stack, and (3) the identification of the Los Chocoyos Ash Layer (Drexler et al., 1980) in the sediment cores. In core ME-27, we have included three additional ^{14}C dates on *N. dutertrei* at 0.5 cm, 80.5 cm, and 125.5 cm depth from Mekik (2014). All radiocarbon ages were calibrated with Calib 7.1 and the marine calibration curve MARINE13 (Reimer et al., 2013; Stuiver & Reimer, 1986), assuming a reservoir age of 467 years as given in Dubois

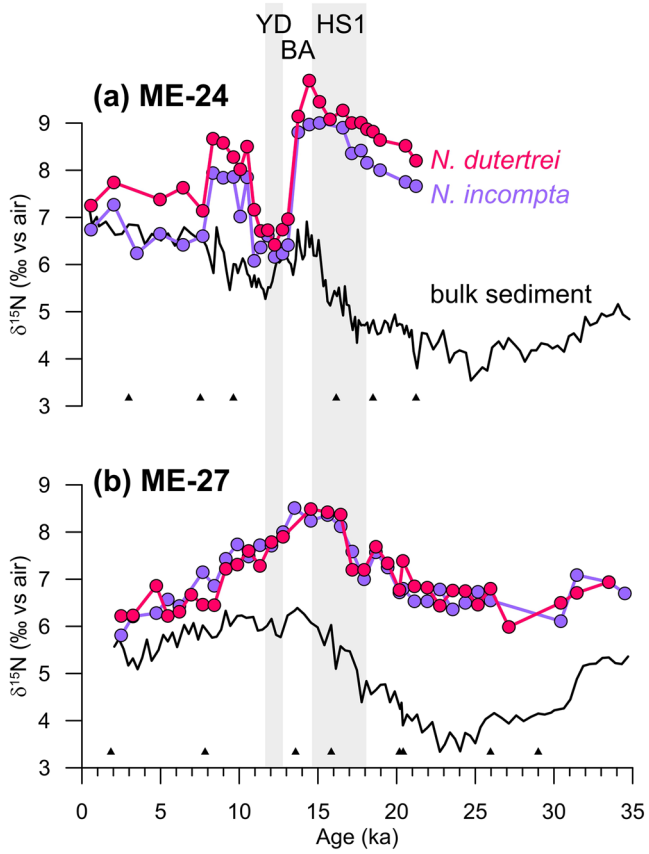

Figure 2. Comparison of $\delta^{15}N$ of foraminifera-bound and bulk sedimentary N in sediment cores ME-24 (a) and ME-27 (b), extending back to 35 ka. FB-$\delta^{15}N$ (this study) is in pink (*N. dutertrei*) and purple (*N. incompta*), and $\delta^{15}N_{bulk}$ (Dubois et al., 2011) is in black. Tie-points are indicated as triangles, and gray shadings highlight the Heinrich Stadial 1 (HS1) and Younger Dryas (YD) intervals.

et al. (2014). Ages were linearly interpolated between the stratigraphic tie points, which are given in Supplementary Table 1.

Foraminifera-bound $\delta^{15}N$ was measured with the "persulfate-denitrifier" technique (Knapp et al., 2005; Ren et al., 2009; Straub et al., 2013). In brief, ~3–5 mg of foraminifera (*N. dutertrei* and *N. incompta* from the 300–600 μm size fraction) were picked, were cut open with a scalpel (rather than being crushed, to minimize sample loss), and underwent a chemical cleaning (Ren et al., 2009; Straub et al., 2013). The organic N bound within the calcite was then released by dissolution with HCl and converted to nitrate in a basic potassium persulfate solution (Nydahl, 1978). The nitrate concentration of the solution was determined by chemiluminescence (Braman & Hendrix, 1989), and an aliquot of the nitrate solution equivalent to 5 nmol N was converted to nitrous oxide (N_2O) by denitrifying bacteria (Sigman et al., 2001). The N isotopic composition of the N_2O was measured with a custom continuous-flow system for N_2O extraction and purification on-line to a Thermo MAT253 stable isotope mass spectrometer and referenced to air N_2 using the international nitrate standards IAEA-N3 and USGS-34 (Weigand et al., 2016). The FB-$\delta^{15}N$ data were then corrected for the contribution of the oxidation procedural blank with an in-house aminocaproic acid standard of known isotopic composition.

After the blank correction, we found linear offsets in FB-$\delta^{15}N$ of up to 0.5–0.6‰ among the individual batches analyzed. The origin of this linear offset may be an additional blank introduced during the cleaning process that was not monitored by the procedural blanks at the time of these analyses. Since we analyzed almost all samples in duplicate across separate batches of analyses, we were able to correct for the artifact by applying offsets to whole batches (Supplementary Figures 1 and 2). Replicate FB-$\delta^{15}N$ analyses for each depth were then averaged, yielding species-specific FB-$\delta^{15}N$ records for both *N. dutertrei* and *N. incompta* in each sediment core. The offset correction does not impact the interpretation of the data.

3. Results

In the $\delta^{15}N_{bulk}$ records measured in ME-24 and ME-27 by Dubois et al. (2011), $\delta^{15}N_{bulk}$ is lowest (4–5‰) during the last ice age, increases to 6–7‰ during the deglaciation, and then slightly increases (ME-24) or decreases (ME-27) during the Holocene (Figure 2).

FB-$\delta^{15}N$ is almost always higher than $\delta^{15}N_{bulk,}$ a common finding when the foraminifera species analyzed lacks dinoflagellate endosymbionts (Martinez-Garcia et al., 2014; Ren et al., 2012; Smart et al., 2018). In terms of downcore change, FB-$\delta^{15}N$ is notably different from $\delta^{15}N_{bulk}$ at both core sites. Most importantly, unlike $\delta^{15}N_{bulk}$, FB-$\delta^{15}N$ during the last ice age (6–8‰) is similar to or higher than that of the late Holocene (6–7.5‰). At both sites, FB-$\delta^{15}N$ gradually increases during deglaciation and shows a deglacial maximum during the HS1 and early Bolling-Allerod (BA). At ME-27, FB-$\delta^{15}N$ then gradually declines throughout the YD and the Holocene. At ME-24, FB-$\delta^{15}N$ declines abruptly during the second half of the BA and is at a minimum during the YD, peaks again during the early Holocene, and then declines into the middle Holocene. Another difference between the two core sites is that at ME-27, FB-$\delta^{15}N$ of *N. dutertrei* and *N. incompta* are very similar, while at ME-24, FB-$\delta^{15}N$ of *N. dutertrei* is on average 0.6‰ higher than FB-$\delta^{15}N$ of *N. incompta*. Despite this difference, the two species show the same down-core changes within each core.

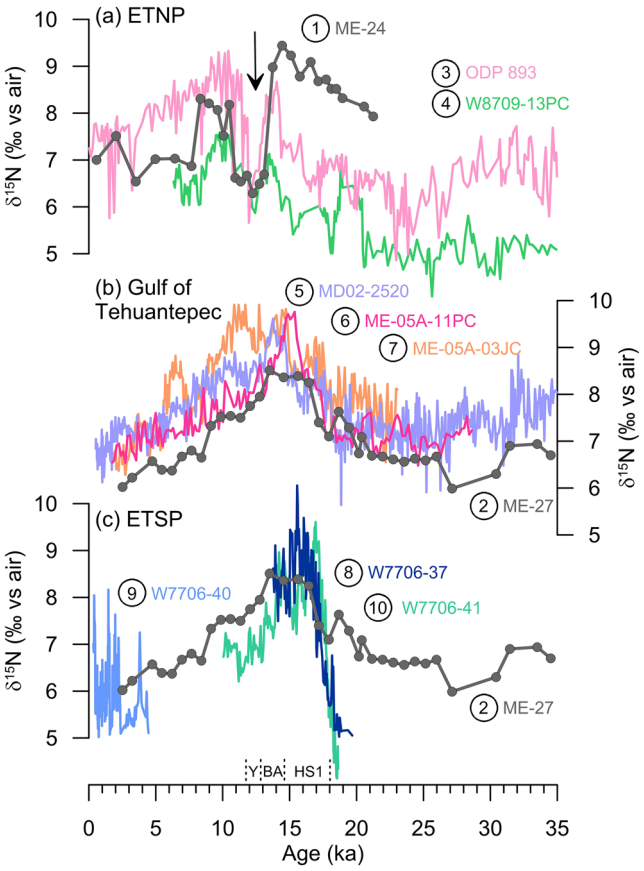

Figure 3. Compilation of bulk sediment $\delta^{15}N$ records from within or proximal to (a) the ETNP denitrification zone, (b) the Gulf of Tehuantepec, and (c) the ETSP denitrification zone, overlain by the FB-$\delta^{15}N$ records of ME-24 (in a) and ME-27 (in b and c). The FB-$\delta^{15}N$ records of *N. dutertrei* and *N. incompta* from each core have been averaged in this figure. Numbers next to cores correspond to those on the maps in Figure 1. Bulk sediment $\delta^{15}N$ data are from: Emmer and Thunell (2000) (ODP 893), S. S. Kienast et al. (2002) (W8709-13PC), Pichevin et al. (2010) (MD02-2520), Hendy and Pedersen (2006) (ME-05A-11PC), Thunell and Kepple (2004) (ME-05A-03JC), and Higginson and Altabet (2004) (W7706-37, -40, and -41).

4. Discussion

4.1. Disagreement Between $\delta^{15}N_{bulk}$ and FB-$\delta^{15}N$

The similarity among the $\delta^{15}N_{bulk}$ records from ME-24 and ME-27 and other cores in the region (Figure 3) appears consistent with a coherent change in nutrient dynamics in the EEP. Furthermore, the location close to the continent and in proximity to two upwelling systems promises high primary productivity that in turn leads to rapid biogenic fluxes and sediment accumulation, which are expected to minimize the influence of diagenetic alteration at the seafloor (Ganeshram et al., 2000; Thunell et al., 2004; Thunell & Kepple, 2004). However, the disagreement with the trends in FB-$\delta^{15}N$ indicates a bias in either $\delta^{15}N_{bulk}$ or FB-$\delta^{15}N$.

More ground-truthing of FB-$\delta^{15}N$ is called for, especially in dynamic environments such as upwelling systems. Observed species-associated offsets point to influences from symbiosis and possibly also from feeding habits, seasonality, and depth habitat (Costa et al., 2016; Ren et al., 2012; Smart et al., 2018, 2020). Moreover, the two species measured here, *N. dutertrei* and *N. incompta*, show an offset in ME-24 of 0.6‰ on average but have no clear offset in ME-27 (Figure 2). *N. dutertrei* are non-spinose and pelagophyte symbiont-bearing, whereas *N. incompta* are non-spinose and asymbiotic (Bird et al., 2018; Takagi et al., 2019). Modern studies indicate that asymbiotic and/or non-spinose species have a distinctly higher FB-$\delta^{15}N$ than spinose, dinoflagellate-bearing species, by as much as 4‰ (Ren et al., 2012; Smart et al., 2018). These studies indicate that pelagophyte symbiont-bearing species, including *N. dutertrei,* cluster with asymbiotic species such as *N. incompta*, consistent with their similar FB-$\delta^{15}N$ in ME-27. We suggest that the $\delta^{15}N$ offset between the two species in ME-24 speaks to a stronger affinity of *N. incompta* for upwelling, which may cause *N. incompta* to be biased toward periods and locations of maximal upwelling, resulting in a lower $\delta^{15}N$ for its food source. Above ME-27, the strong flow of surface waters from the South and their pervasive nutrient-richness may preclude seasonal or small-scale spatial variations in food source $\delta^{15}N$, leading to more similar FB-$\delta^{15}N$ for the two species.

However, a glacial-to-interglacial bias in the FB-$\delta^{15}N$ records is unlikely, lacking a clear mechanism. Supporting this view, the two species show similar changes within each core, including the pronounced $\delta^{15}N$ minimum during late deglaciation in ME-24. Thus, we question the primary nature of the bulk sediment $\delta^{15}N$ records, in particular, their glacial-to-interglacial $\delta^{15}N$ increase. We point to two processes that may bias the bulk sediment $\delta^{15}N$ records to indicate an artificially low $\delta^{15}N$ for sinking N during the last ice age.

First, given the proximity of the South American continent, significant input of organic and inorganic nitrogen from terrestrial sources to the core sites may be occurring. Linear regression of bulk sediment total nitrogen (TN) against total organic carbon (TOC) yields a non-zero intercept (Figure 4a), suggesting the presence of clay-bound N with a low C/N, such as clay-bound ammonium and amino acids (Meckler et al., 2011; Muller et al., 1977; Schubert & Calvert, 2001). If the intercept is entirely due to inorganic N, then it accounts for ~23 ± 14% of the average TN in ME-24 and ME-27. Inorganic N, likely present as ammonium bound in clay minerals, is reported to have a low $\delta^{15}N$, for example, of 2–4‰ (Schubert & Calvert, 2001). The $\delta^{15}N$ of terrestrial organic N probably depends strongly on the region and environment of the source. Nevertheless, given the relatively high $\delta^{15}N$ of marine organic matter in this region, the combined contributions of terrestrial organic and inorganic N would likely work to lower $\delta^{15}N_{bulk}$. $\delta^{15}N_{bulk}$ is indeed mostly lower than FB-$\delta^{15}N$ at both ME-24 and ME-27, even after subtracting 1–2‰ from FB-$\delta^{15}N$ to account for

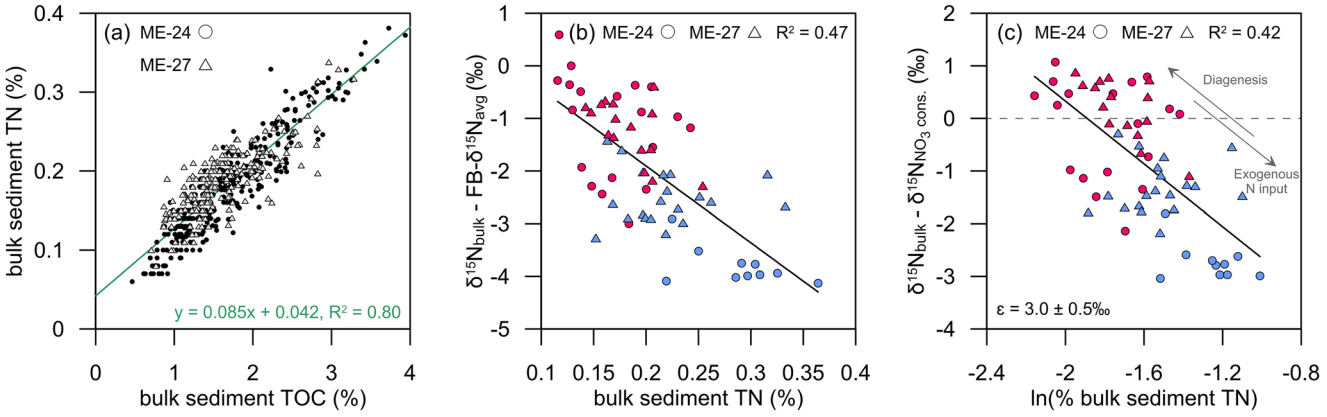

Figure 4. Possible explanations for artificially low bulk sediment $\delta^{15}N$ values in the EEP during the last ice age. (a) In a cross-plot of bulk sediment total N (TN) against total organic carbon (TOC) of sediment cores ME-24 (black circles) and ME-27 (gray triangles), the non-zero *y*-intercept of the trend line suggests the presence of inorganic nitrogen and/or a component of organic matter with a very low C/N. (b) Cross-plot of $\delta^{15}N_{bulk}$–FB-$\delta^{15}N$ against bulk sediment TN of sediment cores ME-24 (circles) and ME-27 (triangles), color-coded for the last ice age and HS1 periods (blue) and the BA period through the Holocene (red). The FB-$\delta^{15}N$ values shown are the two-species averages for each depth. Nitrogen content and N flux (not shown) in ME-24 and ME-27 were higher during the last ice age and HS1 relative to the interglacial, suggesting that a higher fraction of the N flux to the seabed was preserved. This enhanced preservation, in turn, may explain the greater ice age difference between $\delta^{15}N_{bulk}$ and FB-$\delta^{15}N$ as the result of reduced diagenetic elevation of bulk sedimentary $\delta^{15}N$ (i.e., reduced diagenetic N loss) during the last ice age (e.g., due to the lower deep ocean oxygen (Hoogakker et al., 2018)). (c) Following from (b), but with the following modifications. The *y*-axis gives an estimate of the difference between $\delta^{15}N_{bulk}$ and the $\delta^{15}N$ of nitrate consumed (NO_3^- cons.) in the euphotic zone. The latter was calculated from the FB-$\delta^{15}N$ of *N. dutertrei*, from which is subtracted the average difference between the FB-$\delta^{15}N$ of *N. dutertrei* and the $\delta^{15}N$ of euphotic zone nitrate consumed, as observed in a ground-truthing study (1.3 ± 0.6‰; Ren et al., 2012). The *N. incompta* data are not used in (c), due to a lack of surface sediment calibration for this species. The *x*-axis is the natural logarithm of the bulk sediment TN percentage. Assuming the Rayleigh model, the slope of the correlation of $\delta^{15}N$ with ln(%TN) provides an estimate of the net isotope effect for diagenetic N loss of 3.0 ± 0.5‰. In this interpretation, the tendency for $\delta^{15}N_{bulk}$ to be lower than the $\delta^{15}N$ of nitrate consumed in the euphotic zone suggests the background input of low-$\delta^{15}N$ exogenous N to the sediments, as supported by the data in (a).

the typical elevation of asymbiotic and/or non-spinose foraminifera $\delta^{15}N$ relative to the $\delta^{15}N$ of the nitrate consumed in the euphotic zone (Ren et al., 2012; Smart et al., 2018).

Second, weaker diagenetic alteration during the last ice age may have caused or contributed to the glacial-to-interglacial $\delta^{15}N_{bulk}$ difference. The majority of studies indicate that bulk sediment $\delta^{15}N$ increases during oxic organic matter diagenesis (Robinson et al., 2012 and references therein). Oxic diagenesis appears to be strongly affected by oxygen exposure time, which is in turn controlled by bottom water oxygen concentrations, sediment burial rate, and the flux of organic matter to the sediment (Hartnett et al., 1998). Compared to the Holocene, ice age bottom water oxygen concentrations were lower in the deep EEP and ETP, including in the depth range of ME-24 (2941 m) and ME-27 (2203 m) (R. F. Anderson et al., 2019; Bradtmiller et al., 2010; Hoogakker et al., 2018; Jacobel et al., 2020; Loveley et al., 2017). This may have worked to minimize diagenetic loss, and thus, $\delta^{15}N$ elevation, of bulk sedimentary N. Consistent with this possibility, in both ME-24 and ME-27, N content and N flux were higher during the last glacial and HS1 periods relative to the Holocene (Dubois et al., 2011; S. S. Kienast et al., 2007). Moreover, there is a correlation between the difference between $\delta^{15}N_{bulk}$ and FB-$\delta^{15}N$ and the N content of the sediments, with a greater difference between $\delta^{15}N_{bulk}$ and FB-$\delta^{15}N$ during the last glacial (Figure 4b). This is as expected if glacial-age sediment underwent less oxic diagenetic N loss. The slope of correlation in $\delta^{15}N$ against ln(% TN) space provides a Rayleigh model-based estimate of the net isotope effect of diagenesis of 3.0 ± 0.5‰ (Figure 4c) that is consistent with previous estimates (Lehmann et al., 2002; Moebius, 2013). However, we caution that, as discussed above, this trend may alternatively (or additionally) result from exogenous N inputs being more important during the LGM.

4.2. Interpretation of EEP $\delta^{15}N$ Change: Denitrification versus Surface Nitrate Consumption

At EEP sites, both the $\delta^{15}N$ of the nitrate supply and the degree of nitrate consumption may influence the $\delta^{15}N$ of export production. Accordingly, $\delta^{15}N_{bulk}$ records have been scrutinized for changes in both. Differences among EEP records and between EEP and ETP records during deglaciations and interglacials have

been recognized, and these have been interpreted as arising from changes in the degree of nitrate consumption in the EEP (Dubois & Kienast, 2011; Robinson et al., 2009). However, the deglacial $\delta^{15}N_{bulk}$ rise and the higher $\delta^{15}N_{bulk}$ during interglacials are largely shared between the EEP and ETP records (as well as among EEP records), leading to the view that the $\delta^{15}N$ of the nitrate supply in the EEP changes in parallel with the ETP, with water column denitrification being the major driver of these changes (Dubois et al., 2011).

Modern ocean data should provide some insight into the degree to which the EEP should share changes in the $\delta^{15}N$ of the nitrate supply with the ETP. Data from 95°W suggest that the subsurface nitrate being upwelled along the equator has a $\delta^{15}N$ of ~7.1‰ or slightly lower (Rafter et al., 2012; Rafter & Sigman, 2016). At this longitude, the lowest $\delta^{15}N$ of shallow subsurface nitrate is associated with the SSCC, which also underlies the highest nitrate concentrations at the surface. The low nitrate $\delta^{15}N$ of the SSCC likely derives from the remineralization of low-$\delta^{15}N$ sinking N under the region of upwelling (Rafter & Sigman, 2016). These modern observations do not support a dominant role for the intensity of the EUC or other zonal subsurface flows on the $\delta^{15}N$ of subsurface nitrate, at least this far east in the EEP. Rather, the biogeochemical dynamics of the region, both the water column denitrification of the ETP and the incomplete nitrate consumption in the EEP surface, appear to most strongly influence the $\delta^{15}N$ of the nitrate being upwelled in the EEP. On the basis of prior studies of equatorial circulation and biogeochemical dynamics, a similar interpretation was put forward by Robinson et al. (2009). Thus, EEP sites should detect a significant reduction in ETP denitrification during the LGM. Such an influence is even more likely east of the Galapagos, due to the proximity to the suboxic zones and the interference of the islands with the eastward subsurface flows along the equator. In summary, modern ocean data support prior interpretations of shared $\delta^{15}N_{bulk}$ changes among EEP and ETP records as deriving from changes in ETP denitrification.

Thus, based in part on the evidence above, the deglacial rise and Holocene elevation of bulk sediment $\delta^{15}N$ from ME-24 and ME-27 have been interpreted as dominantly reflecting reduced water column denitrification during the LGM relative to the Holocene (Dubois et al., 2011), consistent with the previous conclusion of such a change on the basis of non-equatorial ETP records (Emmer & Thunell, 2000; Ganeshram et al., 2000, 1995; S. S. Kienast et al., 2002; Robinson et al., 2009). From this perspective, the FB-$\delta^{15}N$ records, lacking such an LGM-to-Holocene $\delta^{15}N$ difference, would appear to cast doubt on this overarching interpretation of an LGM reduction in ETP denitrification. We address this question next.

4.3. LGM-to-Holocene History of ETP Water Column Denitrification

As discussed in the prior section, the low glacial $\delta^{15}N_{bulk}$ observed at both ETP and EEP sites has been interpreted as a reduction in water column denitrification during the last ice age (Dubois et al., 2011; Dubois & Kienast, 2011; Emmer & Thunell, 2000; Ganeshram et al., 2000, 1995; S. S. Kienast et al., 2002; Robinson et al., 2009). However, not all $\delta^{15}N_{bulk}$ records in the ETP indicate an LGM-to-Holocene $\delta^{15}N$ rise. For example, $\delta^{15}N_{bulk}$ records from the Gulf of Tehuantepec indicate a deglacial maximum in $\delta^{15}N$ but no glacial-to-interglacial change, consistent with the FB-$\delta^{15}N$ measurements (Figure 3b; Hendy & Pedersen, 2006; Pichevin et al., 2010; Pride et al., 1999; Thunell & Kepple, 2004). More broadly, in specific records from both further North and South in the ETP, bulk sediment $\delta^{15}N$ is observed to return to glacial values over the Holocene (Figure 3a,c; Emmer & Thunell, 2000; Higginson & Altabet, 2004; S. S. Kienast et al., 2002; Pride et al., 1999). Thus, the FB-$\delta^{15}N$ data are not alone in casting doubt on an LGM-to-Holocene rise in $\delta^{15}N$ in the ETP and EEP. We propose that the "true" $\delta^{15}N$ signal for the ETP is a deglacial maximum, with the low glacial $\delta^{15}N$ observed at some ETP sites being a consequence of higher exogenous N input and/or reduced diagenetic alteration during the ice ages.

Suggested explanations for the gradual Holocene decline in $\delta^{15}N_{bulk}$ have ranged widely, including a decline in ETP water column denitrification, a rise in N_2 fixation, and/or a decline in mean ocean nitrate $\delta^{15}N$ (Deutsch et al., 2004; Galbraith et al., 2013; Thunell & Kepple, 2004). In other proxies that are sensitive to suboxia, the dominant signal appears to be of a deglacial maximum in ETP suboxia, rather than a secular rise in suboxia from the last glacial to the interglacial (Hendy & Pedersen, 2006; Hoogakker et al., 2018; Y. Zheng et al., 2000). These data favor the interpretation of a deglacial maximum in ETP water column denitrification, with the possibility that denitrification rates were comparable between the LGM and the late Holocene. However, other records suggest a more durable shift to suboxia (Chang et al., 2014; Muratli et al., 2010).

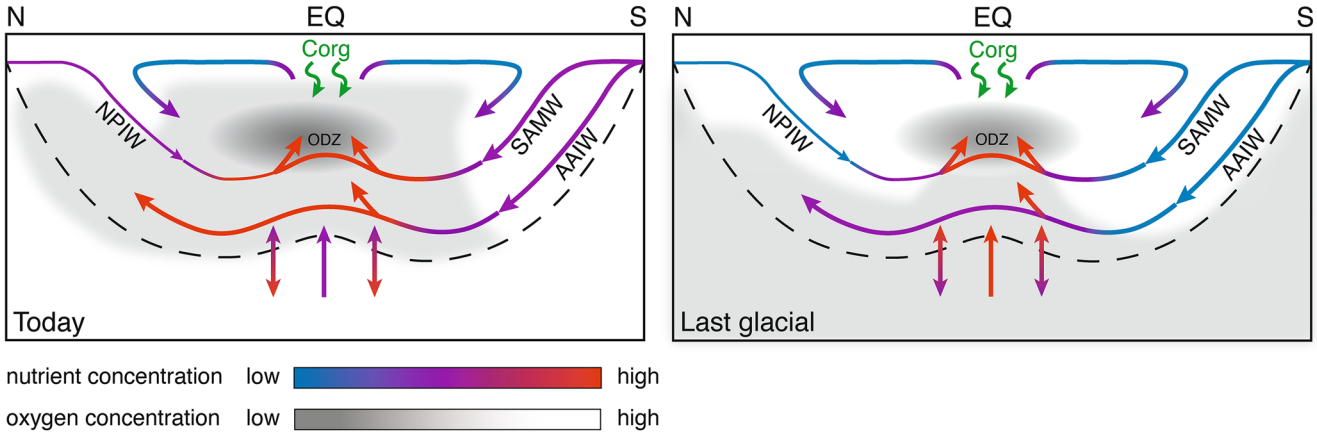

Figure 5. Schematic cross section of the low latitude upper ocean today and during the last glacial period, highlighting the counteracting effects on the oxygen-deficient zones (ODZs) of the eastern tropical Pacific during the last ice age. The colored arrows and lines indicate the nutrient (i.e., phosphate and nitrate) concentration of waters supplied by advection (unidirectional arrows) or by mixing (bidirectional arrows). The gray shading is darker for lower oxygen concentration, with the two ODZs (of the ETNP and ETSP) shown as a single ODZ for simplicity. NPIW, North Pacific Intermediate Water; SAMW, Subantarctic Mode Water; AAIW, Antarctic Intermediate Water. The FB-$\delta^{15}N$ data reported in this study raise the possibility that water column denitrification rates in the ETP were similar during the last glacial period and today. Colder temperatures and lower preformed nutrient concentrations of intermediate waters (SAMW and AAIW) would have worked against the development of ODZs during the last ice age. However, the lower O_2 concentration of the deep ocean and its mixing with and upwelling into the tropical thermocline would have fostered ODZ development. It is possible that these opposing mid-depth and deep ocean forcings offset one another to yield similar ODZ extent in the LGM and Holocene (see text). The implied lack of change in export production (C_{org}) is uncertain but appears appropriate for the easternmost equatorial Pacific (Costa et al., 2017).

Addressing this question further is warranted from multiple perspectives. First, the history of ETP water column denitrification is central to the operation of the global ocean N budget over glacial cycles. Second, denitrification reflects thermocline suboxia, the extent of which is an important aspect of the ocean's environmental conditions. Third, the extent of suboxia is impacted by ocean circulation and the cycling of carbon and nutrients; thus, it provides an important constraint on changes in these processes over the glacial cycles. Next, we consider the plausibility that ETP suboxia was similar between the LGM and the latter Holocene, in comparison to the prevailing interpretation that suboxia was reduced during the LGM.

4.4. Suboxia in the EEP and ETP During the Last Ice Age

The interpretation of a reduction in ETP water column denitrification during ice ages has been argued to be consistent with expectations given other characteristics of the ice age ocean (Galbraith et al., 2004). First, the water ventilating the thermocline was colder during the LGM, increasing preformed O_2 concentrations. Second, arguments have been made for faster thermocline ventilation during the ice ages (Galbraith et al., 2004). Third, enhanced nutrient consumption in polar and subpolar surface waters would have worked to reduce the preformed nutrient concentration of the thermocline, tending to reduce low latitude biological productivity and the rate of oxygen consumption from the respiration of the resulting sinking organic matter (Figure 5; Keir, 1988; Robinson et al., 2005; Sigman and Boyle, 2000). Finally, North Atlantic overturning has alternated between North Atlantic Deep Water (NADW) formation during interglacials and Glacial North Atlantic Intermediate Water (GNAIW) formation during glacials (Oppo & Lehman, 1993). In most configurations of their downstream circulations, switching from NADW to GNAIW works to raise mid-depth O_2 concentrations (Boyle, 1988; Hain et al., 2010; Sigman et al., 2003).

However, countering these changes is the evidence that the ocean's biological pump was more efficient during the ice ages. Broecker (1982a, b) first proposed a stronger global ocean biological pump as the cause of the lowering of atmospheric CO_2 during the last ice age. He recognized that such a strengthening in the biological pump should also have caused a decline in the average O_2 concentration of the ocean interior. Indeed, there is now strong evidence for lower O_2 in the glacial deep ocean (R. F. Anderson et al., 2019; Bradtmiller et al., 2010; François et al., 1997; Galbraith and Jaccard, 2015; Hoogakker et al., 2018; Jaccard et al., 2016, 2009; Jaccard and Galbraith, 2012; Jacobel et al., 2020; Loveley et al., 2017; Marcantonio

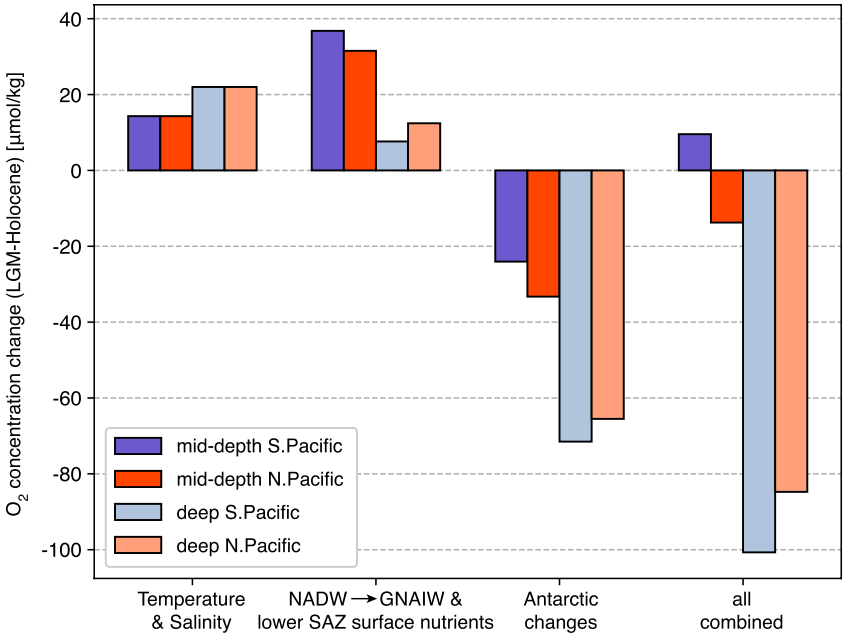

Figure 6. Estimates of contributors to oxygen (O_2) concentration changes in the Pacific during the Last Glacial Maximum relative to the Holocene, based on solubility changes as well as CYCLOPS box model results of Hain et al. (2010). From left to right, the four sets of bars show the following. (left) Changes in O_2 solubility (Garcia and Gordon, 1992) caused by cooling from 14°C-to-11°C and 4°C-to-1°C in the mid-depth and deep Pacific, respectively, combined with a whole-ocean salinity increase from 34.7 to 35.7. (Center left) Simulated changes in O_2 utilization when glacial shoaling of the AMOC (GNAIW replacing NADW circulation; see Sigman et al., 2003) is combined with more complete surface nutrient consumption in the Subantarctic (SAZ) responding to iron fertilization, reducing the preformed nutrient concentration of the waters ventilating the mid-depths (see Martinez-Garcia et al., 2014; Robinson et al., 2005). (Center right) Simulated changes in O_2 utilization in response to two changes in the Antarctic Zone: reduced exchange between the deep Southern Ocean and the Antarctic surface combined with more complete Antarctic surface nutrient consumption (Ai et al., 2020; François et al., 1997; Kemeny et al., 2018; Sigman et al., 2021; Studer et al., 2015; Wang et al., 2017). (Right) Sum of O_2 solubility change and simulated O_2 utilization change when all model forcings are combined to represent the LGM (Hain et al., 2010). O_2 utilization is calculated using O_2:$P_{regenerated}$ of −170:1 (L. A. Anderson and Sarmiento, 1994). The indication of this analysis is that there were counteracting influences on the O_2 concentration of the mid-depth Pacific during the LGM. On the one hand, AMOC shoaling, Subantarctic iron fertilization and cooling would have increased O_2 concentrations in the mid-depth and deep Pacific. On the other hand, the above-described Antarctic changes would have made the global biological pump more efficient, raising the concentration of regenerated nutrients and causing a major decline in the O_2 concentration in most of the global ocean interior, especially the deep ocean but also the mid-depth Pacific through vertical exchange and/or deep upwelling. The net result of these combined changes is a strong decline in O_2 concentration in the deep Pacific and relatively minor predicted O_2 changes in the mid-depth Pacific during the LGM. "All combined" does not equal a simple summation of the component changes, due to interactions among the components. For example, the effect of the switch from NADW to GNAIW on ocean interior O_2 depends on the degree of nutrient drawdown at the Antarctic surface. For further context, description of the model scenarios described here, and detailed analysis of simulated carbon cycle and atmospheric CO_2 changes, see Hain et al. (2010).

et al., 2020). This glacial decline in deep ocean O_2, through mixing and diffuse interior upwelling, would also have worked to lower the O_2 concentration in overlying mid-depth waters (Figure 5).

To gain insight into these competing influences on mid-depth O_2, we turn to output from a geochemical box model that has been used to investigate the potential causes of the ice age reduction in atmospheric CO_2 (Hain et al., 2010). Here, we focus on the model-indicated sensitivities of O_2 in the model's deep and mid-depth South and North Pacific boxes (Figure 6). Considering first the solubility effects of an ice age ocean that was 3°C colder and 1 PSU saltier than modern, the ocean interior oxygen concentration increases modestly, by 14 µmol/kg at mid-depths and 22 µmol/kg in the deep ocean (Garcia & Gordon, 1992). The combined effects of Subantarctic iron fertilization (which reduced the nutrient content of Subantarctic surface water and Subantarctic Mode Water; Martinez-Garcia et al., 2014; Robinson et al., 2005) and the shift from NADW to GNAIW (Lynch-Stieglitz et al., 2007) cause a reduction in regenerated nutrient burden

and O_2 utilization in the Pacific that translates to an additional and more substantial rise in mid-depth O_2. However, further strengthening of the ocean's biological pump through an increase in the degree of nutrient consumption in Antarctic surface waters as well as a decline in Antarctic overturning (Ai et al., 2020; François et al., 1997; Sigman et al., 2021; Studer et al., 2015; Wang et al., 2017) leads to a buildup of regenerated nutrients and a strong decline in deep ocean O_2, consistent with available O_2 reconstructions (see above) and indicative of a more efficient global biological pump (Hain et al., 2014). The circulation communicates some of this O_2 decline to the mid-depth Pacific boxes as well. Combining this full list of ice age changes, the net result is little change in mid-depth Pacific O_2 concentration (Figure 6). In short, increasing the efficiency of the global ocean's biological pump so as to lower atmospheric CO_2 to ice age observations tends to offset other influences on mid-depth O_2, calling for little difference in mid-depth O_2 between the LGM and the Holocene.

These large-scale impacts having been considered, we must recognize that changes in ODZ extent and volume may be partially decoupled from average mid-depth O_2 concentration. In addition to being affected by the preformed O_2 and nutrient concentrations and the rate of newly forming intermediate waters, the ODZs may be sensitive to the spatial pattern of thermocline ventilation and the wind-driven upwelling of thermocline waters into the surface, the former delivering O_2 and the latter causing focused O_2 consumption. However, there is as yet no clarity as to how these smaller scale processes would have changed between the LGM and the Holocene.

4.5. Deglacial Features

In the two cores studied, both bulk sediment and foraminifera-bound $\delta^{15}N$ show deglacial features (Figure 2); we focus here on the shell-bound data. Our first concern is the overall deglacial $\delta^{15}N$ maximum shared by the two records (Figure 2), which is also observed in many low latitude bulk sediment $\delta^{15}N$ records within and beyond the ETP (Figure 3). Previous work suggests that the $\delta^{15}N$ maximum includes both a global thermocline signal and an ETP-specific deglacial maximum in water column denitrification (e.g., De Pol-Holz, 2006; Deutsch et al., 2004; Galbraith et al., 2013; Hendy & Pedersen, 2006; Y. Zheng et al., 2000). These and other studies propose a range of plausible explanations for these global and/or local deglacial maxima. However, while the FB-$\delta^{15}N$ records reported here are not completely clear on the point, there is a suggestion that the $\delta^{15}N$ rise begins before the deglaciation. If so, this adds to a body of data suggesting that the EEP "deglacial" signal actually includes a change preceding deglaciation (M. Kienast et al., 2006). One possibility is a response to orbitally (e.g., precession) driven insolation change (Rafter & Charles, 2012).

Another possible origin for the putative deglacial peak in ETP suboxia, which may also explain its early onset, involves apparently distinct timings for different Southern Ocean changes. In the Subantarctic, the indicators of iron fertilization appear to begin their declines early in the deglaciation (Martinez-Garcia et al., 2014; Wang et al., 2017). In addition, ocean warming began quite early in the deglacial sequence (Bereiter et al., 2018). In contrast, the Antarctic surface "isolation" of the LGM appears to decrease somewhat later and more gradually, continuing through the deglaciation and Holocene (Ai et al., 2020; Wang et al., 2017). As outlined above, the Antarctic deglacial change should have caused a deglacial decline in suboxia while the other two (Subantarctic and temperature) deglacial changes should have caused a deglacial rise in suboxia (Figure 6). Accordingly, the relative timing of these components may be appropriate to have caused a deglacial/early Holocene peak in suboxia and thus in ETP/EEP nitrate $\delta^{15}N$. Evaluation of this hypothesis awaits additional records with strong chronological controls.

While our two records both share an overall deglacial $\delta^{15}N$ maximum, there are significant differences between the FB-$\delta^{15}N$ records from ME-24 and ME-27. The clearest distinction is the FB-$\delta^{15}N$ minimum of ME-24 centered on the Younger Dryas. The two sediment cores are separated by only 2° of latitude and 4° of longitude (Figure 1). However, ME-24 is located immediately above the equator, where the $\delta^{15}N$ of this subsurface nitrate may have a greater sensitivity to changes in denitrification in the ETNP (Rafter et al., 2012; Rafter & Sigman, 2016). ME-27, on the other hand, is located under the influence of the coastal upwelling off Peru as well as in the broad region of southern hemisphere-biased open ocean upwelling of the EEP (Figure 1) and may thus be more sensitive to changes in denitrification in the ETSP (Dubois et al., 2011, 2014; Robinson et al., 2009).

The Younger Dryas FB-$\delta^{15}N$ minimum in ME-24 is accompanied by similar $\delta^{15}N$ minima in bulk sediment records from the ETNP (Figure 3a; Emmer & Thunell, 2000; Hendy et al., 2004; S. S. Kienast et al., 2002), also coinciding with metal redox indicators of higher ETNP thermocline oxygen at this time (Cartapanis et al., 2011; Chang et al., 2014; Hendy & Pedersen, 2005; Y. Zheng et al., 2000). We thus tentatively interpret the $\delta^{15}N$ minimum as the result of lower nitrate $\delta^{15}N$ in the subsurface waters of ME-24, resulting from a reduction in ETNP denitrification. Consistent with this interpretation, the lack of such a minimum in ME-27 matches its corresponding lack in bulk sediment $\delta^{15}N$ records from the ETSP margin of Peru and Chile (Figure 3c; Higginson & Altabet, 2004).

As for the physical cause of this putative YD decline in ETNP denitrification, one possibility is a southward shift in the Intertropical Convergence Zone (ITCZ) during the YD, driven by northern hemisphere cooling at the time (Lea et al., 2003). Such a shift may have reduced upwelling along the EEP as a result of reduced cross-equatorial southeast trade winds (Koutavas & Lynch-Stieglitz, 2005), decreasing denitrification in the ETNP. However, this fails to explain why a similar event did not occur during HS1, when there was also abrupt northern hemisphere cooling (Bond et al., 1993). Indeed, it appears that HS1 was associated with higher, not lower, upwelling in the EEP (M. Kienast et al., 2006), which has been explained as the result of intensified northeast trade winds during HS1 when the ITCZ appears to have been at its southernmost position (S. S. Kienast et al., 2013; Timmermann et al., 2007). These conflicts encourage consideration of larger scale causes for the putative YD decline in ETNP denitrification. In this category, a cooling-associated acceleration of North Pacific thermocline ventilation has been suggested for the YD (Mikolajewicz et al., 1997).

In our interpretation of the deglacial changes, we have assigned primary signal to bulk sediment $\delta^{15}N$ records. Further above, the disagreement of bulk sediment and foraminifera-bound $\delta^{15}N$ in ME-24 and ME-27 was interpreted to argue against a primary origin for the glacial/interglacial $\delta^{15}N$ difference in bulk sediment. We do not see these interpretations as contradictory. In some cases, down-core changes in bulk sediment $\delta^{15}N$ will dominantly reflect the primary isotopic signal of the N sinking out of the surface ocean; in other cases, bulk sediment $\delta^{15}N$ and its changes may be heavily altered by exogenous N or changes in diagenesis. The latter case is most likely when substantial changes in sedimentary environment occur, such as between glacial and interglacial intervals (Meckler et al., 2011).

5. Conclusions

In two sediment cores from the EEP, we measured foraminifera-bound $\delta^{15}N$ back to ~35 ka during the last ice age. FB-$\delta^{15}N$ values are similar during the Holocene and the last glacial, unlike bulk sedimentary $\delta^{15}N$, which is lower during the Last Glacial Maximum (LGM) relative to the Holocene. Our FB-$\delta^{15}N$ data do not appear to agree with previous bulk sediment-based inferences of reduced water column denitrification during the last ice age. Instead, our FB-$\delta^{15}N$ data imply similar rates of water column denitrification during the Holocene and the last glacial and thus no dramatic LGM-to-Holocene change in suboxia in the ETP. Mechanisms have previously been identified for reduced ETP suboxia during the ice ages (e.g., Galbraith et al., 2004). We suggest that these were offset by the documented ice age decline in oxygen concentration in the deep Pacific waters underlying the Pacific thermocline. Mixing with, and upwelling from, these deeper less-well oxygenated waters would have helped to maintain the suboxic zones during the ice ages (Figure 5).

We caution that the observation of lower bulk sediment $\delta^{15}N$ during the LGM extends both northward and southward along the eastern Pacific margin (De Pol-Holz et al., 2006; Galbraith et al., 2004; Ganeshram et al., 2000; Hendy et al., 2004; S. S. Kienast et al., 2002; Robinson et al., 2007), and our data do not directly test the veracity of these higher latitude bulk sediment $\delta^{15}N$ records. Moreover, in part due to our lack of spatial coverage, we have been unable to assess the possible role of variations in the degree of nutrient consumption in the reconstructed $\delta^{15}N$ changes, and yet, core-top bulk sediment $\delta^{15}N$ and FB-$\delta^{15}N$ data indicate that this is a potentially significant variable in the nutrient-rich EEP (Costa et al., 2016; Farrell et al., 1995). In addition, the rate at which undercurrent and countercurrent waters are imported from the west could also change. As discussed above, modern ocean data argue against this as a major driver of $\delta^{15}N$ change, but it cannot be ruled out. Finally, mean ocean nitrate $\delta^{15}N$ may have changed from the LGM to the deglaciation, and then through the Holocene (Galbraith et al., 2013). In net, the potential for overlapping of signals leaves open the possibility that the LGM-Holocene similarity in EEP FB-$\delta^{15}N$ does not reflect similar

extents of suboxia during the LGM and Holocene. Generating additional FB-$\delta^{15}N$ records from the ETP suboxic zones will not address all uncertainties; nevertheless, this is the obvious next step.

Data Availability Statement

Data from this study are deposited at the PANGAEA repository (https://doi.pangaea.de/10.1594/PANGAEA.925339).

Acknowledgments
We acknowledge June Padman, Maziet Cheseby and Alan Mix for providing us with samples from the core archives at the University of Oregon. We thank Alexa Weigand for her help and advice with laboratory analyses. Funding for the N isotope work was provided by the Swiss National Science Foundation grant PBEZP2_145695 to A.S.S, US National Science Foundation grants 0922345, 1060947, and 1401489 to D.M.S. We thank Rebecca Robinson and an anonymous reviewer for their comments, which improved the manuscript. Open access funding enabled and organized by Projekt DEAL.

References

Ai, X. E., Studer, A. S., Sigman, D. M., Martínez-García, A., Fripiat, F., Thöle, L. M., et al. (2020). Southern Ocean upwelling, Earth's obliquity, and glacial-interglacial atmospheric CO_2 change. *Science*, *370*(6522), 1348–1352. https://doi.org/10.1126/science.abd2115

Altabet, M. A. (2001). Nitrogen isotopic evidence for micronutrient control of fractional NO_3- utilization in the equatorial pacific. *Limnology & Oceanography*, *46*(2), 368–380.

Altabet, M. A., & François, R. (1994). Sedimentary nitrogen isotopic ratio as a recorder for surface ocean nitrate utilization. *Global Biogeochemical Cycles*, *8*(1), 103–116. https://doi.org/10.1029/93GB03396

Altabet, M. A., François, R., Murray, D., & Prell, W. (1995). Climate-related variations in denitrification in the Arabian Sea from sediment N-15/N-14 ratios. *Nature*, *373*(6514), 506–509. https://doi.org/10.1038/373506a0

Altabet, M. A., Higginson, M. J., & Murray, D. W. (2002). The effect of millennial-scale changes in Arabian Sea denitrification on atmospheric CO_2. *Nature*, *415*(6868), 159–162. https://doi.org/10.1038/415159a

Anderson, L. A., & Sarmiento, J. L. (1994). Redfield ratios of remineralization determined by nutrient data analysis. *Global Biogeochemical Cycles*, *8*(1), 65–80. https://doi.org/10.1029/93GB03318

Anderson, R. F., Sachs, J. P., Fleisher, M. Q., Allen, K. A., Yu, J., Koutavas, A., & Jaccard, S. L. (2019). Deep-sea oxygen depletion and ocean carbon sequestration during the last ice age. *Global Biogeochemical Cycles*, *33*(3), 301–317. https://doi.org/10.1029/2018GB006049

Bereiter, B., Shackleton, S., Baggenstos, D., Kawamura, K., & Severinghaus, J. (2018). Mean global ocean temperatures during the last glacial transition. *Nature*, *553*(7686), 39–44. https://doi.org/10.1038/nature25152

Bird, C., Darling, K. F., Russell, A. D., Fehrenbacher, J. S., Davis, C. V., Free, A., & Ngwenya, B. T. (2018). 16S rRNA gene metabarcoding and TEM reveals different ecological strategies within the genus Neogloboquadrina (planktonic foraminifer). *PloS One*, *13*(1), e0191653. https://doi.org/10.1371/journal.pone.0191653

Bond, G., Broecker, W., Johnsen, S., Mcmanus, J., Labeyrie, L., Jouzel, J., & Bonani, G. (1993). Correlations between climate records from North-Atlantic sediments and Greenland ice. *Nature*, *365*(6442), 143–147. https://doi.org/10.1038/365143a0

Boyle, E. (1988). The role of vertical chemical fractionation in controlling late quaternary atmospheric carbon-dioxide. *Journal of Geophysical Research-Oceans*, *93*(C12), 15701–15714. https://doi.org/10.1029/JC093iC12p15701

Bradtmiller, L. I., Anderson, R. F., Sachs, J. P., & Fleisher, M. Q. (2010). A deeper respired carbon pool in the glacial equatorial Pacific Ocean. *Earth and Planetary Science Letters*, *299*(3), 417–425. https://doi.org/10.1016/j.epsl.2010.09.022

Braman, R., & Hendrix, S. (1989). Nanogram nitrite and nitrate determination in environmental and biological-materials by vanadium(III) reduction with chemiluminescence detection. *Analytical Chemistry*, *61*(24), 2715–2718. https://doi.org/10.1021/ac00199a007

Broecker, W. (1982a). Glacial to interglacial changes in ocean chemistry. *Progress in Oceanography*, *11*(2), 151–197. https://doi.org/10.1016/0079-6611(82)90007-6

Broecker, W. (1982b). Ocean chemistry during glacial time. *Geochimica et Cosmochimica Acta*, *46*(10), 1689–1705. https://doi.org/10.1016/0016-7037(82)90110-7

Cartapanis, O., Tachikawa, K., & Bard, E. (2011). Northeastern Pacific oxygen minimum zone variability over the past 70 kyr: Impact of biological production and oceanic ventilation. *Paleoceanography*, *26*, PA4208. https://doi.org/10.1029/2011PA002126

Chang, A. S., Pedersen, T. F., & Hendy, I. L. (2008). Late Quaternary paleoproductivity history on the Vancouver Island margin, western Canada: A multiproxy geochemical study. *Canadian Journal of Earth Sciences 45*, 1283–1297. https://doi.org/10.1139/E08-038

Chang, A. S., Pedersen, T. F., & Hendy, I. L. (2014). Effects of productivity, glaciation, and ventilation on late Quaternary sedimentary redox and trace element accumulation on the Vancouver Island margin, western Canada. *Paleoceanography*, *29*(7), 730–746. https://doi.org/10.1002/2013PA002581

Cline, J. D., & Kaplan, I. R. (1975). Isotopic fractionation of dissolved nitrate during denitrification in the eastern tropical north Pacific Ocean. *Marine Chemistry*, *3*(4), 271–299. https://doi.org/10.1016/0304-4203(75)90009-2

Costa, K. M., Jacobel, A. W., McManus, J. F., Anderson, R. F., Winckler, G., & Thiagarajan, N. (2017). Productivity patterns in the equatorial Pacific over the last 30,000 years. *Global Biogeochemical Cycles*, *31*(5), 850–865. https://doi.org/10.1002/2016GB005579

Costa, K. M., McManus, J. F., Anderson, R. F., Ren, H., Sigman, D. M., Winckler, G., et al. (2016). No iron fertilization in the equatorial Pacific Ocean during the last ice age. *Nature*, *529*(7587), 519. https://doi.org/10.1038/nature16453

Darling, K. F., Kucera, M., Kroon, D., & Wade, C. M. (2006). A resolution for the coiling direction paradox in *Neogloboquadrina pachyderma*. *Paleoceanography*, *21*(2), PA2011. https://doi.org/10.1029/2005PA001189

De Pol-Holz, R., Robinson, R. S., Hebbeln, D., Sigman, D. M., & Ulloa, O. (2009). Controls on sedimentary nitrogen isotopes along the Chile margin. *Deep-Sea Research Part II-Topical Studies in Oceanography*, *56*(16), 1100–1112. https://doi.org/10.1016/j.dsr2.2008.09.014

De Pol-Holz, R., Ulloa, O., Dezileau, L., Kaiser, J., Lamy, F., & Hebbeln, D. (2006). Melting of the Patagonian ice sheet and deglacial perturbations of the nitrogen cycle in the eastern South Pacific. *Geophysical Research Letters*, *33*(4), L04704. https://doi.org/10.1029/2005GL024477

De Pol-Holz, R., Ulloa, O., Lamy, F., Dezileau, L., Sabatier, P., & Hebbeln, D. (2007). Late Quaternary variability of sedimentary nitrogen isotopes in the eastern South Pacific Ocean. *Paleoceanography*, *22*(2). https://doi.org/10.1029/2006PA001308

Deutsch, C., Gruber, N., Key, R. M., Sarmiento, J. L., & Ganachaud, A. (2001). Denitrification and N_2 fixation in the Pacific Ocean. *Global Biogeochemical Cycles*, *15*(2), 483–506. https://doi.org/10.1029/2000GB001291

Deutsch, C., Sigman, D. M., Thunell, R. C., Meckler, A. N., & Haug, G. H. (2004). Isotopic constraints on glacial/interglacial changes in the oceanic nitrogen budget. *Global Biogeochemical Cycles*, *18*(4), GB4012. https://doi.org/10.1029/2003GB002189

Drexler, J. W., Rose, W. I., Sparks, R. S. J., & Ledbetter, M. T. (1980). The Los Chocoyos Ash, Guatemala: A major stratigraphic marker in middle America and in three ocean basins. *Quaternary Research*, *13*(3), 327–345. https://doi.org/10.1016/0033-5894(80)90061-7

Dubois, N., & Kienast, M. (2011). Spatial reorganization in the equatorial divergence in the eastern tropical Pacific during the last 150 kyr. *Geophysical Research Letters*, *38*, L16606. https://doi.org/10.1029/2011GL048325

Dubois, N., Kienast, M., Kienast, S., Normandeau, C., Calvert, S. E., Herbert, T. D., & Mix, A. (2011). Millennial-scale variations in hydrography and biogeochemistry in the Eastern Equatorial Pacific over the last 100 kyr. *Quaternary Science Reviews*, *30*(1–2), 210–223. https://doi.org/10.1016/j.quascirev.2010.10.012

Dubois, N., Kienast, M., Kienast, S. S., & Timmermann, A. (2014). Millennial-scale Atlantic/East Pacific sea surface temperature linkages during the last 100,000 years. *Earth and Planetary Science Letters*, *396*, 134–142. https://doi.org/10.1016/j.epsl.2014.04.008

Emmer, E., & Thunell, R. C. (2000). Nitrogen isotope variations in Santa Barbara Basin sediments: Implications for denitrification in the eastern tropical North Pacific during the last 50,000 years. *Paleoceanography*, *15*(4), 377–387. https://doi.org/10.1029/1999PA000417

Farrell, J., Pedersen, T., Calvert, S., & Nielsen, B. (1995). Glacial-interglacial changes in nutrient utilization in the Equatorial Pacific-Ocean. *Nature*, *377*(6549), 514–517. https://doi.org/10.1038/377514a0

François, R., Altabet, M. A., Yu, E. F., Sigman, D. M., Bacon, M. P., Frank, M., et al. (1997). Contribution of Southern Ocean surface-water stratification to low atmospheric CO_2 concentrations during the last glacial period. *Nature*, *389*(6654), 929–935. https://doi.org/10.1038/40073

Galbraith, E. D., & Jaccard, S. L. (2015). Deglacial weakening of the oceanic soft tissue pump: Global constraints from sedimentary nitrogen isotopes and oxygenation proxies. *Quaternary Science Reviews*, *109*, 38–48. https://doi.org/10.1016/j.quascirev.2014.11.012

Galbraith, E. D., Kienast, M., Albuquerque, A. L., Altabet, M. A., Batista, F., Bianchi, D., et al. (2013). The acceleration of oceanic denitrification during deglacial warming. *Nature Geoscience*, *6*(7), 579–584. https://doi.org/10.1038/NGEO1832

Galbraith, E. D., Kienast, M., Pedersen, T. F., & Calvert, S. E. (2004). Glacial-interglacial modulation of the marine nitrogen cycle by high-latitude O_2 supply to the global thermocline. *Paleoceanography*, *19*(4), PA4007. https://doi.org/10.1029/2003PA001000

Ganeshram, R. S., Pedersen, T., Calvert, S., & Murray, J. (1995). Large changes in oceanic nutrient inventories from glacial to interglacial periods. *Nature*, *376*(6543), 755–758. https://doi.org/10.1038/376755a0

Ganeshram, R. S., Pedersen, T. F., Calvert, S. E., McNeill, G. W., & Fontugne, M. R. (2000). Glacial-interglacial variability in denitrification in the world's oceans: Causes and consequences. *Paleoceanography*, *15*(4), 361–376. https://doi.org/10.1029/1999PA000422

Garcia, H. E., & Gordon, L. (1992). Oxygen solubility in seawater—Better fitting equations. *Limnology & Oceanography*, *37*(6), 1307–1312. https://doi.org/10.4319/lo.1992.37.6.1307

Garcia, H. E., Locarnini, R. A., Boyer, T. P., Antonov, J. I., Zweng, M. M., Baranova, O. K., & Johnson, D. R. (2010). World Ocean Atlas 2009, Volume 4: Nutrients (phosphate, nitrate, silicate). In S. Levitus (Ed.), Ed., *NOAA Atlas NESDIS 71* (p. 398). U.S. Government Printing Office. https://www.nodc.noaa.gov/OC5/WOA09/pubwoa09.html

Goodman, P. J., Hazeleger, W., De Vries, P., & Cane, M. (2005). Pathways into the Pacific Equatorial undercurrent: A trajectory analysis. *Journal of Physical Oceanography*, *35*(11), 2134–2151. https://doi.org/10.1175/JPO2825.1

Hain, M. P., Sigman, D. M., & Haug, G. H. (2010). Carbon dioxide effects of Antarctic stratification, North Atlantic intermediate water formation, and subantarctic nutrient drawdown during the last ice age: Diagnosis and synthesis in a geochemical box model. *Global Biogeochemical Cycles*, *24*, GB4023. https://doi.org/10.1029/2010GB003790

Hain, M. P., Sigman, D. M., & Haug, G. H. (2014). The Biological pump in the past. *Treatise on Geochemistry*. 2nd ed., Vol. 8, chapter 18, 485–517. https://doi.org/10.1016/B978-0-08-095975-7.00618-5

Hartnett, H. E., Keil, R. G., Hedges, J. I., & Devol, A. H. (1998). Influence of oxygen exposure time on organic carbon preservation in continental margin sediments. *Nature*, *391*(6667), 572–574. https://doi.org/10.1038/35351

Hendy, I. L., & Pedersen, T. F. (2005). Is pore water oxygen content decoupled from productivity on the California Margin? Trace element results from Ocean Drilling Program Hole 1017E, San Lucia slope, California. *Paleoceanography*, *20*(4), PA4026. https://doi.org/10.1029/2004PA001123

Hendy, I. L., & Pedersen, T. F. (2006). Oxygen minimum zone expansion in the eastern tropical North Pacific during deglaciation. *Geophysical Research Letters*, *33*(20), L20602. https://doi.org/10.1029/2006GL025975

Hendy, I. L., Pedersen, T. F., Kennett, J. P., & Tada, R. (2004). Intermittent existence of a southern Californian upwelling cell during submillennial climate change of the last 60 kyr. *Paleoceanography*, *19*(3), PA3007. https://doi.org/10.1029/2003PA000965

Higginson, M. J., & Altabet, M. A. (2004). Initial test of the silicic acid leakage hypothesis using sedimentary biomarkers. *Geophysical Research Letters*, *31*(18), L18303. https://doi.org/10.1029/2004GL020511

Hoogakker, B. A. A., Lu, Z., Umling, N., Jones, L., Zhou, X., Rickaby, R. E. M., et al. (2018). Glacial expansion of oxygen-depleted seawater in the eastern tropical Pacific. *Nature*, *562*(7727), 410. https://doi.org/10.1038/s41586-018-0589-x

Jaccard, S. L., & Galbraith, E. D. (2012). Large climate-driven changes of oceanic oxygen concentrations during the last deglaciation. *Nature Geoscience*, *5*(2), 151–156. https://doi.org/10.1038/NGEO1352

Jaccard, S. L., Galbraith, E. D., Martinez-Garcia, A., & Anderson, R. F. (2016). Covariation of deep Southern Ocean oxygenation and atmospheric CO_2 through the last ice age. *Nature*, *530*(7589), 207. https://doi.org/10.1038/nature16514

Jaccard, S. L., Galbraith, E. D., Sigman, D. M., Haug, G. H., François, R., Pedersen, T. F., et al. (2009). Subarctic Pacific evidence for a glacial deepening of the oceanic respired carbon pool. *Earth and Planetary Science Letters*, *277*(1–2), 156–165. https://doi.org/10.1016/j.epsl.2008.10.017

Jacobel, A. W., Anderson, R. F., Jaccard, S. L., McManus, J. F., Pavia, F. J., & Winckler, G. (2020). Deep Pacific storage of respired carbon during the last ice age: Perspectives from bottom water oxygen reconstructions. *Quaternary Science Reviews*, *230*, 106065. https://doi.org/10.1016/j.quascirev.2019.106065

Keir, R. S. (1988). On the Late Pleistocene ocean geochemistry and circulation. *Paleoceanography*, *3*(4), 413–445. https://doi.org/10.1029/PA003i004p00413

Kemeny, P. C., Kast, E. R., Hain, M. P., Fawcett, S. E., Fripiat, F., Studer, A. S., et al. (2018). A seasonal model of nitrogen isotopes in the ice age Antarctic zone: Support for weakening of the Southern Ocean upper overturning cell. *Paleoceanography and Paleoclimatology*, *33*(12), 1453–1471. https://doi.org/10.1029/2018PA003478

Kessler, W. S. (2006). The circulation of the eastern tropical Pacific: A review. *Progress in Oceanography*, *69*(2–4), 181–217. https://doi.org/10.1016/j.pocean.2006.03.009

Kienast, M., Kienast, S. S., Calvert, S. E., Eglinton, T. I., Mollenhauer, G., François, R., & Mix, A. C. (2006). Eastern Pacific cooling and Atlantic overturning circulation during the last deglaciation. *Nature*, *443*(7113), 846–849. https://doi.org/10.1038/nature05222

Kienast, S. S., Calvert, S. E., & Pedersen, T. F. (2002). Nitrogen isotope and productivity variations along the northeast Pacific margin over the last 120 kyr: Surface and subsurface paleoceanography. *Paleoceanography*, *17*(4), 1055. https://doi.org/10.1029/2001PA000650

Kienast, S. S., Friedrich, T., Dubois, N., Hill, P. S., Timmermann, A., Mix, A. C., & Kienast, M. (2013). Near collapse of the meridional SST gradient in the eastern equatorial Pacific during Heinrich Stadial 1. *Paleoceanography*, *28*(4), 663–674. https://doi.org/10.1002/2013PA002499

Kienast, S. S., Kienast, M., Mix, A. C., Calvert, S. E., & François, R. (2007). Thorium-230 normalized particle flux and sediment focusing in the Panama Basin region during the last 30,000 years. *Paleoceanography*, *22*(2), PA2213. https://doi.org/10.1029/2006PA001357

Knapp, A. N., Sigman, D. M., & Lipschultz, F. (2005). N isotopic composition of dissolved organic nitrogen and nitrate at the Bermuda Atlantic time-series study site. *Global Biogeochemical Cycles*, *19*(1), GB1018. https://doi.org/10.1029/2004GB002320

Koutavas, A., & Lynch-Stieglitz, J. (2005). Variability of the marine ITCZ over the eastern Pacific during the past 30,000 years—Regional perspective and global context. In H. F. Diaz & R. S. Bradley (Eds.), Eds., *Hadley circulation: Present, past and future* (Vol. 21, pp. 347–369). Springer. https://doi.org/10.1007/978-1-4020-2944-8_12

Kusch, S., Eglinton, T. I., Mix, A. C., & Mollenhauer, G. (2010). Timescales of lateral sediment transport in the Panama Basin as revealed by radiocarbon ages of alkenones, total organic carbon and foraminifera. *Earth and Planetary Science Letters*, *290*(3–4), 340–350. https://doi.org/10.1016/j.epsl.2009.12.030

Lea, D. W., Pak, D. K., Peterson, L. C., & Hughen, K. A. (2003). Synchroneity of tropical and high-latitude Atlantic temperatures over the last glacial termination. *Science*, *301*(5638), 1361–1364. https://doi.org/10.1126/science.1088470

Lehmann, M. F., Bernasconi, S. M., Barbieri, A., & McKenzie, J. A. (2002). Preservation of organic matter and alteration of its carbon and nitrogen isotope composition during simulated and in situ early sedimentary diagenesis. *Geochimica et Cosmochimica Acta*, *66*(20), 3573–3584. https://doi.org/10.1016/S0016-7037(02)00968-7

Liu, K., & Kaplan, I. (1989). The eastern Tropical Pacific as a source of N-15-enriched nitrate in seawater off Southern-California. *Limnology & Oceanography*, *34*(5), 820–830. https://doi.org/10.4319/lo.1989.34.5.0820

Loveley, M. R., Marcantonio, F., Wisler, M. M., Hertzberg, J. E., Schmidt, M. W., & Lyle, M. (2017). Millennial-scale iron fertilization of the eastern equatorial Pacific over the past 100,000 years. *Nature Geoscience*, *10*(10), 760–764. https://doi.org/10.1038/ngeo3024

Lukas, R. (1986). The termination of the equatorial undercurrent in the eastern Pacific. *Progress in Oceanography*, *16*(2), 63–90. https://doi.org/10.1016/0079-6611(86)90007-8

Lynch-Stieglitz, J., Adkins, J. F., Curry, W. B., Dokken, T., Hall, I. R., Herguera, J. C., et al. (2007). Atlantic meridional overturning circulation during the last glacial maximum. *Science*, *316*(5821), 66–69. https://doi.org/10.1126/science.1137127

Marcantonio, F., Hostak, R., Hertzberg, J. E., & Schmidt, M. W. (2020). Deep Equatorial Pacific Ocean oxygenation and atmospheric CO_2 over the last ice age. *Scientific Reports*, *10*(1), 6606. https://doi.org/10.1038/s41598-020-63628-x

Martinez-Garcia, A., Sigman, D. M., Ren, H., Anderson, R. F., Straub, M., Hodell, D. A., et al. (2014). Iron fertilization of the Subantarctic Ocean during the last ice age. *Science*, *343*(6177), 1347–1350. https://doi.org/10.1126/science.1246848

Martinez, P., Lamy, F., Robinson, R. R., Pichevin, L., & Billy, I. (2006). Atypical delta N-15 variations at the southern boundary of the East Pacific oxygen minimum zone over the last 50 ka. *Quaternary Science Reviews*, *25*(21–22), 3017–3028. https://doi.org/10.1016/j.quascirev.2006.04.009

Meckler, A. N., Ren, H., Sigman, D. M., Gruber, N., Plessen, B., Schubert, C. J., & Haug, G. H. (2011). Deglacial nitrogen isotope changes in the Gulf of Mexico: Evidence from bulk sedimentary and foraminifera-bound nitrogen in Orca Basin sediments. *Paleoceanography*, *26*, PA4216. https://doi.org/10.1029/2011PA002156

Mekik, F. (2014). Radiocarbon dating of planktonic foraminifer shells: A cautionary tale. *Paleoceanography*, *29*(1), 13–29. https://doi.org/10.1002/2013PA002532

Mikolajewicz, U., Crowley, T. J., Schiller, A., & Voss, R. (1997). Modelling teleconnections between the North Atlantic and North Pacific during the Younger Dryas. *Nature*, *388*(6642), 602–602. https://doi.org/10.1038/41595

Moebius, J. (2013). Isotope fractionation during nitrogen remineralization (ammonification): Implications for nitrogen isotope biogeochemistry. *Geochimica et Cosmochimica Acta*, *105*, 422–432. https://doi.org/10.1016/j.gca.2012.11.048

Muller, P. (1977). C-N ratios in Pacific deep-sea sediments—Effect of inorganic ammonium and organic nitrogen-compounds sorbed by clays. *Geochimica et Cosmochimica Acta*, *41*(6), 765–776. https://doi.org/10.1016/0016-7037(77)90047-3

Muratli, J. M., Chase, Z., Mix, A. C., & McManus, J. (2010). Increased glacial-age ventilation of the Chilean margin by Antarctic intermediate water. *Nature Geoscience*, *3*(1), 23–26.

Nydahl, F. (1978). Peroxodisulfate oxidation of total nitrogen in waters to nitrate. *Water Research*, *12*(12), 1123–1130. https://doi.org/10.1016/0043-1354(78)90060-X

Oppo, D., & Lehman, S. (1993). Mid-depth circulation of the subpolar North-Atlantic during the last glacial maximum. *Science*, *259*(5098), 1148–1152. https://doi.org/10.1126/science.259.5098.1148

Peters, B. D., Lam, P. J., & Casciotti, K. L. (2018). Nitrogen and oxygen isotope measurements of nitrate along the US GEOTRACES Eastern Pacific Zonal Transect (GP16) yield insights into nitrate supply, remineralization, and water mass transport. *Marine Chemistry*, *201*, 137–150. https://doi.org/10.1016/j.marchem.2017.09.009

Pichevin, L. E., Ganeshram, R. S., Francavilla, S., Arellano-Torres, E., Pedersen, T. F., & Beaufort, L. (2010). Interhemispheric leakage of isotopically heavy nitrate in the eastern tropical Pacific during the last glacial period. *Paleoceanography*, *25*, PA1204. https://doi.org/10.1029/2009PA001754

Pierotti, D., & Rasmussen, R. (1980). Nitrous-oxide measurements in the Eastern Tropical Pacific-Ocean. *Tellus*, *32*(1), 56–72.

Pride, C., Thunell, R., Sigman, D., Keigwin, L., Altabet, M., & Tappa, E. (1999). Nitrogen isotopic variations in the Gulf of California since the last deglaciation: Response to global climate change. *Paleoceanography*, *14*(3), 397–409. https://doi.org/10.1029/1999PA900004

Rafter, P. A., & Charles, C. D. (2012). Pleistocene equatorial Pacific dynamics inferred from the zonal asymmetry in sedimentary nitrogen isotopes. *Paleoceanography*, *27*, PA3102. https://doi.org/10.1029/2012PA002367

Rafter, P. A., & Sigman, D. M. (2016). Spatial distribution and temporal variation of nitrate nitrogen and oxygen isotopes in the upper equatorial Pacific Ocean. *Limnology & Oceanography*, *61*(1), 14–31. https://doi.org/10.1002/lno.10152

Rafter, P. A., Sigman, D. M., Charles, C. D., Kaiser, J., & Haug, G. H. (2012). Subsurface tropical Pacific nitrogen isotopic composition of nitrate: Biogeochemical signals and their transport. *Global Biogeochemical Cycles*, *26*, GB1003. https://doi.org/10.1029/2010GB003979

Reimer, P. J., Bard, E., Bayliss, A., Beck, J. W., Blackwell, P. G., Ramsey, C. B., et al. (2013). Intcal13 and Marine13 radiocarbon age calibration curves 0–50,000 years Cal Bp. *Radiocarbon*, *55*(4), 1869–1887. https://doi.org/10.2458/azu_js_rc.55.16947

Ren, H., Sigman, D. M., Meckler, A. N., Plessen, B., Robinson, R. S., Rosenthal, Y., & Haug, G. H. (2009). Foraminiferal isotope evidence of reduced nitrogen fixation in the ice age Atlantic Ocean. *Science*, *323*(5911), 244–248. https://doi.org/10.1126/science.1165787

Ren, H., Sigman, D. M., Thunell, R. C., & Prokopenko, M. G. (2012). Nitrogen isotopic composition of planktonic foraminifera from the modern ocean and recent sediments. *Limnology & Oceanography*, *57*(4), 1011–1024. https://doi.org/10.4319/lo.2012.57.4.1011

Robinson, R. S., Brunelle, B. G., & Sigman, D. M. (2004). Revisiting nutrient utilization in the glacial Antarctic: Evidence from a new method for diatom-bound N isotopic analysis. *Paleoceanography*, *19*(3), PA3001. https://doi.org/10.1029/2003PA000996

Robinson, R. S., Kienast, M., Albuquerque, A. L., Altabet, M., Contreras, S., De Pol Holz, R., et al. (2012). A review of nitrogen isotopic alteration in marine sediments. *Paleoceanography*, *27*, PA4203. https://doi.org/10.1029/2012PA002321

Robinson, R. S., Martinez, P., Pena, L. D., & Cacho, I. (2009). Nitrogen isotopic evidence for deglacial changes in nutrient supply in the eastern equatorial Pacific. *Paleoceanography*, *24*, PA4213. https://doi.org/10.1029/2008PA001702

Robinson, R. S., Mix, A., & Martinez, P. (2007). Southern Ocean control on the extent of denitrification in the southeast Pacific over the last 70 ka. *Quaternary Science Reviews*, *26*(1–2), 201–212. https://doi.org/10.1016/j.quascirev.2006.08.005

Robinson, R. S., Sigman, D. M., DiFiore, P. J., Rohde, M. M., Mashiotta, T. A., & Lea, D. W. (2005). Diatom-bound N-15/N-14: New support for enhanced nutrient consumption in the ice age subantarctic. *Paleoceanography*, *20*(3), PA3003. https://doi.org/10.1029/2004PA001114

Schlitzer, R. (2002). Interactive analysis and visualization of geoscience data with ocean data view. *Computers & Geosciences*, *28*(10), 1211–1218. https://doi.org/10.1016/S0098-3004(02)00040-7

Schubert, C. J., & Calvert, S. E. (2001). Nitrogen and carbon isotopic composition of marine and terrestrial organic matter in Arctic Ocean sediments: Implications for nutrient utilization and organic matter composition. *Deep-Sea Research Part I-Oceanographic Research Papers*, *48*(3), 789–810. https://doi.org/10.1016/S0967-0637(00)00069-8

Sigman, D. M., & Boyle, E. A. (2000). Glacial/interglacial variations in atmospheric carbon dioxide. *Nature*, *407*(6806), 859–869. https://doi.org/10.1038/35038000

Sigman, D. M., Casciotti, K. L., Andreani, M., Barford, C., Galanter, M., & Bohlke, J. K. (2001). A bacterial method for the nitrogen isotopic analysis of nitrate in seawater and freshwater. *Analytical Chemistry*, *73*(17), 4145–4153. https://doi.org/10.1021/ac010088e

Sigman, D. M., DiFiore, P. J., Hain, M. P., Deutsch, C., & Karl, D. M. (2009). Sinking organic matter spreads the nitrogen isotope signal of pelagic denitrification in the North Pacific. *Geophysical Research Letters*, *36*, L08605. https://doi.org/10.1029/2008GL035784

Sigman, D. M., Fripiat, F., Studer, A. S., Kemeny, P. C., Martínez-García, A., Hain, M. P., et al. (2021). The Southern Ocean during the ice ages: A review of the Antarctic surface isolation hypothesis, with comparison to the North Pacific. *Quaternary Science Reviews*, *254*, 106732. https://doi.org/10.1016/j.quascirev.2020.106732

Sigman, D. M., Granger, J., DiFiore, P. J., Lehmann, M. M., Ho, R., Cane, G., & van Geen, A. (2005). Coupled nitrogen and oxygen isotope measurements of nitrate along the eastern North Pacific margin. *Global Biogeochemical Cycles*, *19*(4), GB4022. https://doi.org/10.1029/2005GB002458

Sigman, D. M., Lehman, S. J., & Oppo, D. W. (2003). Evaluating mechanisms of nutrient depletion and C-13 enrichment in the intermediate-depth Atlantic during the last ice age. *Paleoceanography*, *18*(3), 1072. https://doi.org/10.1029/2002PA000818

Silva, N., & Neshyba, S. (1979). On the southernmost extension of the Peru-Chile undercurrent. *Deep Sea Research Part A. Oceanographic Research Papers*, *26*(12), 1387–1393. https://doi.org/10.1016/0198-0149(79)90006-2

Smart, S. M., Fawcett, S. E., Ren, H., Schiebel, R., Tompkins, E. M., Martínez-García, A., et al. (2020). The nitrogen isotopic composition of tissue and shell-bound organic matter of planktic foraminifera in Southern Ocean surface waters. *Geochemistry, Geophysics, Geosystems*, *21*(2), e2019GC008440. https://doi.org/10.1029/2019GC008440

Smart, S. M., Ren, H., Fawcett, S. E., Schiebel, R., Conte, M., Rafter, P. A., et al. (2018). Ground-truthing the planktic foraminifer-bound nitrogen isotope paleo-proxy in the Sargasso Sea. *Geochimica et Cosmochimica Acta*, *235*, 463–482. https://doi.org/10.1016/j.gca.2018.05.023

Straub, M., Sigman, D. M., Ren, H., Martinez-Garcia, A., Meckler, A. N., Hain, M. P., & Haug, G. H. (2013). Changes in North Atlantic nitrogen fixation controlled by ocean circulation. *Nature*, *501*(7466), 200. https://doi.org/10.1038/nature12397

Studer, A. S., Sigman, D. M., Martinez-Garcia, A., Benz, V., Winckler, G., Kuhn, G., et al. (2015). Antarctic Zone nutrient conditions during the last two glacial cycles. *Paleoceanography*, *30*(7), 845–862. https://doi.org/10.1002/2014PA002745

Stuiver, M., & Reimer, P. (1986). A computer-program for radiocarbon age calibration. *Radiocarbon*, *28*(2B), 1022–1030. https://doi.org/10.1017/S0033822200060276

Takagi, H., Kimoto, K., Fujiki, T., Saito, H., Schmidt, C., Kucera, M., & Moriya, K. (2019). Characterizing photosymbiosis in modern planktonic foraminifera. *Biogeosciences*, *16*(17), 3377–3396. https://doi.org/10.5194/bg-16-3377-2019

Talley, L. D., Pickard, G. L., Emery, W. J., & Swift, J. H. (2011). *Descriptive physical oceanography*. Elsevier. https://doi.org/10.1016/C2009-0-24322-4

Thunell, R. C., & Kepple, A. B. (2004). Glacial-holocene delta N-15 record from the Gulf of Tehuantepec, Mexico: Implications for denitrification in the eastern equatorial Pacific and changes in atmospheric N_2O. *Global Biogeochemical Cycles*, *18*(1), GB1001. https://doi.org/10.1029/2002GB002028

Thunell, R. C., Sigman, D. M., Muller-Karger, F., Astor, Y., & Varela, R. (2004). Nitrogen isotope dynamics of the Cariaco Basin, Venezuela. *Global Biogeochemical Cycles*, *18*(3), GB3001. https://doi.org/10.1029/2003GB002185

Timmermann, A., Okumura, Y., An, S.-I., Clement, A., Dong, B., Guilyardi, E., et al. (2007). The influence of a weakening of the Atlantic meridional overturning circulation on ENSO. *Journal of Climate*, *20*(19), 4899–4919. https://doi.org/10.1175/JCLI4283.1

Wang, X. T., Sigman, D. M., Prokopenko, M. G., Adkins, J. F., Robinson, L. F., Hines, S. K., et al. (2017). Deep-sea coral evidence for lower Southern Ocean surface nitrate concentrations during the last ice age. *Proceedings of the National Academy of Sciences of the United States of America*, *114*(13), 3352–3357. https://doi.org/10.1073/pnas.1615718114

Weigand, M. A., Foriel, J., Barnett, B., Oleynik, S., & Sigman, D. M. (2016). Updates to instrumentation and protocols for isotopic analysis of nitrate by the denitrifier method. *Rapid Communications in Mass Spectrometry*, *30*(12), 1365–1383. https://doi.org/10.1002/rcm.7570

Wyrtki, K. (1966). Oceanography of the eastern Equatorial Pacific Ocean. *Oceanography and Marine Biology an Annual Review*, *4*, 33–68.

Zheng, S., Feng, M., Du, Y., Cheng, X., & Li, J. (2016). Annual and interannual variability of the tropical instability vortices in the Equatorial Eastern Pacific observed from Lagrangian surface drifters. *Journal of Climate*, *29*(24), 9163–9177. https://doi.org/10.1175/JCLI-D-16-0124.1

Zheng, Y., van Geen, A., Anderson, R. F., Gardner, J. V., & Dean, W. E. (2000). Intensification of the northeast Pacific oxygen minimum zone during the Bolling-Allerod warm period. *Paleoceanography*, *15*(5), 528–536. https://doi.org/10.1029/1999PA000473